

8D.7 GENESIS OF TYPHOON FENGSHEN (2008) FROM VORTEX SUPERPOSITION: PALAU FIELD EXPERIMENT AND A GLOBAL CLOUD-RESOLVING SIMULATION

Hiroyuki Yamada¹, Tomoe Nasuno¹, Wataru Yanase²,
Ryuichi Shirooka¹, and Masaki Satoh^{2,1}

¹Japan Agency for Marine-Earth Science and Technology, Yokosuka, Japan

²Atmosphere and Ocean Research Institute, University of Tokyo, Kashiwa, Japan

1. INTRODUCTION

One of the greatest remaining challenges in the study of tropical cyclone is to understand and predict their formation from weak cyclonic disturbances. In the western tropical Pacific, although many previous studies pointed out the participation of large- and synoptic-scale cyclonic disturbances in tropical cyclogenesis (e.g., Sobel and Bretherton 1999; Dickinson and Molinari 2002; Fu et al. 2007), little is known about mechanisms governing their transformation into a deep warm-core vortex. In considerable part, the lack of understanding in this area stems from a lack of observation over the ocean. Moreover, insufficient computer resource that limits horizontal domain of numerical models prevents performing a cloud-resolving simulation of multiscale processes ranging from convective to large scale. To overcome these problems, we carried out a field experiment with two Doppler radars in the Pacific warm pool, and applied a state-of-the-art global cloud-resolving model with 3.5 km of horizontal resolution to a case study of Typhoon Fengshen (2008) that formed in the experimental region (Fig. 1a). In this paper, we describe synoptic- and convective-scale processes leading to the formation of a deep upright typhoon vortex, based on results of both the observation and simulation. The main emphasis of this study falls on a role of the superposition of two synoptic-scale vortices on tropical cyclogenesis.

2. OBSERVATION AND SIMULATION

The field experiment was carried out from 1 June through 15 July 2008, as an enhanced observational phase of a JAMSTEC's research project titled "Pacific area long-term atmospheric observation for understanding climate change (PALAU)." As indicated in Fig. 1a, a X-band ground-based radar was placed in the Republic of Palau (134.5°E, 7.4°N), while a C-band ship-borne Doppler radar was mounted on the research vessel *Mirai* that was stayed at (135.0°E, 12.0°N). Each of radar performed a full-volume scan out to 150 km range every 10 minutes, in addition to a surveillance scan every 30 minutes at 0.5° elevation angle with a maximum range of 300 km.

Corresponding author address: Hiroyuki Yamada
JAMSTEC, yamada@jamstec.go.jp

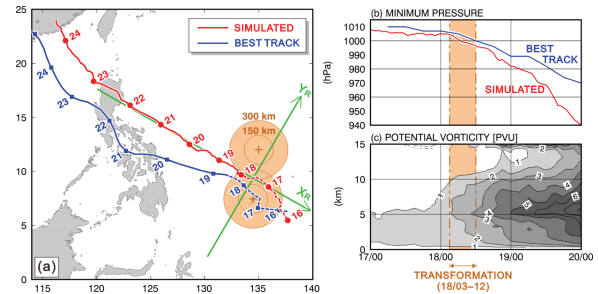


Figure 1. (a) The observed and simulated tracks of Typhoon Fengshen. The 150-km and 300-km ranges of Doppler radars are shown by orange circles. Axes of the rotated Cartesian (X_R - Y_R) coordinates are drawn by green arrows. (b) Time series of the minimum pressure at surface. (c) A time-height plot of the potential vorticity, averaged within 100-km radius from the surface vortex center. The period in which the incipient surface vortex transformed into a deep typhoon vortex (i.e., 0300–1200 UTC 18 June) is highlighted. Time is represented by date/hour.

The global cloud-resolving simulation was conducted using the Nonhydrostatic Icosahedral Atmospheric Model (NICAM), which was designed for fine-mesh [$O(1\text{km})$] global simulations including explicit moist processes in a nonhydrostatic framework (Satoh et al. 2008). The model domain covers the whole globe with 3.5-km horizontal resolution. An advantage of using the global model is to eliminate lateral boundaries that sometimes exert artificial influences upon the propagation of waves and disturbances possessing mesoscale convective systems. The simulation was initialized using the European Centre for Medium-Range Weather Forecasts (ECMWF)—Year of Tropical Convection (YOTC) operational data (with horizontal resolution of $0.5^\circ \times 0.5^\circ$) at 0000 UTC 15 June 2008, which was four days prior to the designation of Fengshen as a tropical storm.

3. SYNOPTIC-SCALE EVOLUTION

The overall evolution of the simulated surface vortex is marked by its formation in the Doppler radar observational area (Fig. 1a) and the start of pressure fall in the period 0300–1200 UTC 18 June (Fig. 1b), which are consistent with the

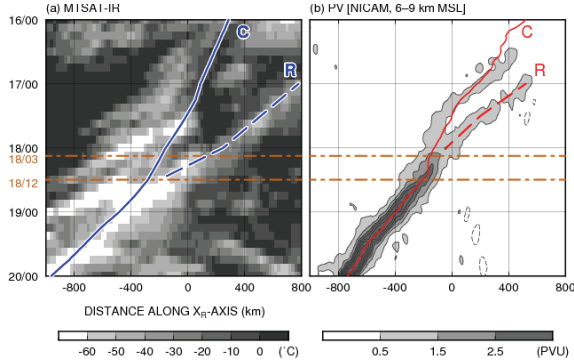


Figure 2. Time-distance plots of (a) the infrared cloud-top temperature observed by the JMA MTSAT geostationary satellite and (b) the simulated potential vorticity averaged between 6 and 9 km MSL, along X_R -axis in the rotated coordinates. Location of the surface vortex center (C) and the mid-tropospheric vortex (R) are highlighted.

characteristics of the observed counterpart. The simulated vortex is also characterized by a rapid increase in the potential vorticity in the middle troposphere (Fig. 1c). The Hovmöller diagram of potential vorticity (Fig. 2b) in the rotated (X_R - Y_R) coordinates (see Fig. 1a) indicates that the potential vorticity started to increase after two vorticity maxima (labeled “C” and “R”) merged together. In the observation (Fig. 2a), this phenomenon can be identified as the merger of two cloud systems above the surface vortex center. Figure 3 illustrates the simulated merger process in the vertical cross sections along X_R -axis. In 17 June, two areas of positive vorticity existed separately, with different height of the peak value: a peak in C below 5 km while a peak in R near 7 km. The rear-side peak R superposed upon the surface vortex C (Fig. 3c), and a single upright vortex subsequently intensified. Thus, these sections clearly represent that the superposition of the mid-tropospheric vorticity peak caused the transformation of the preexisting surface vortex into a deep upright vortex. Although this superposition was not observed, the separated state before superposition was captured by the Doppler radar at the Palau Islands (Fig. 4a). The time-height plot of horizontal winds, derived from the Velocity Azimuth Display (VAD) analysis (Mapes and Lin 2005), shows the passage of two cyclonic wind shifts in different height. They correspond to the two vortices (C and R), as also identified from the similar plot using simulated wind data in the similar domain (Fig. 4b). Therefore, both the observation and simulation provide evidence that Typhoon Fengsen formed

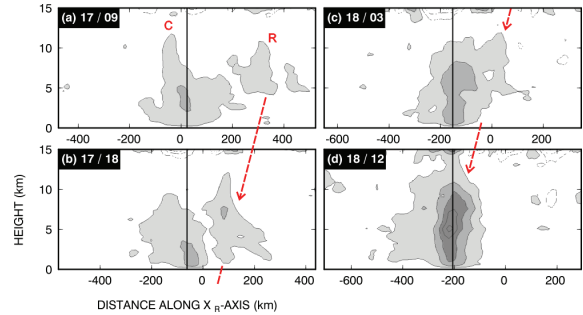


Figure 3. The 9-hourly horizontal-vertical plots of the simulated positive vorticity along X_R -axis. Contours and gray shades are drawn in the same manner as Fig. 2b.

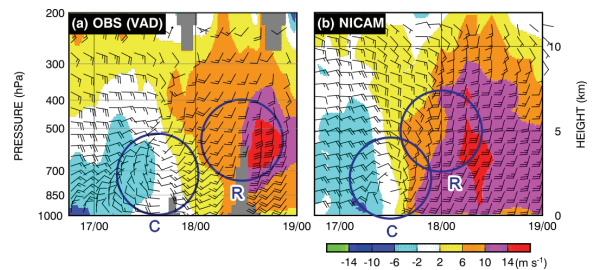


Figure 4. The time-height plots of meridional wind component (color) and wind bars, (a) derived from the VAD analysis using Doppler velocity data within a 60-km circle from the Palau radar, and (b) simulated by NICAM and averaged within a 60-km radius.

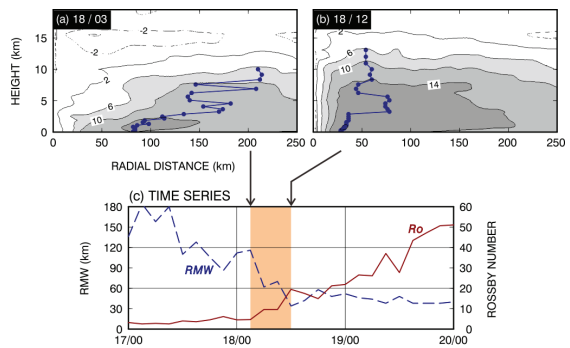


Figure 5. (a and b) The radius-height plots of the azimuthally-averaged tangential winds before and after the transformation. Solid circles connected by a line indicate RMW at each layer. (c) Time series of RMW and Rossby number (Ro).

through the superposition of two synoptic-scale vortices.

Next, the vertical structure of the simulated surface vortex (C) before and after the transformation is illustrated by the traditional radius-height plot of the azimuthally-averaged tangential winds (Figs. 5a and b). It is clearly seen

that the shallow and loose incipient circulation was deepened and tightened dramatically in the inner core region (≤ 100 km). Time series of the radius of maximum tangential wind (RMW), averaged between 0 and 5 km MSL (a broken line in Fig. 5c), indicates that the RMW decreased until 1200 UTC 18 June, and kept almost constant value (40–50 km) after the transformation. To examine the transition of force balance in the surface vortex center, Rossby number (Ro) was measured using the RMW and maximum tangential wind, as follows.

$$Ro = V_{MAX} / (f \times RMW)$$

Here, f is Coriolis parameter. In the time series (Fig. 5c), Ro was less than 10 before the transformation and increased dramatically to a value of several tens (i.e., $Ro \gg 1$) after this. The increase in Ro suggests that the inner-core rotation was initially in gradient-wind balance and subsequently shifted to cyclostrophic wind balance, associated with the establishment of the deep and compact typhoon circulation.

4. CONVECTIVE-SCALE PROCESS DURING VORTEX SUPERPOSITION

The simulation also reproduced a significant change in the structure of convective clouds and vorticity distribution within the inner core region associated with the vortex superposition (Fig. 6). Before the superposition (0000UTC 18 June, left

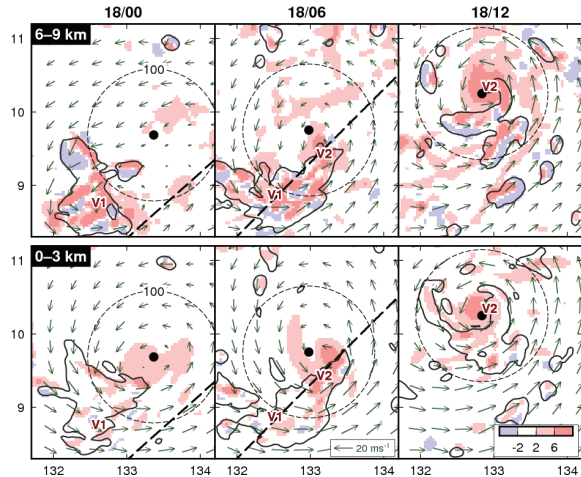


Figure 6. The 6-hourly horizontal distributions of the system-relative wind vectors, potential vorticity (color, in PVU), and hydrometeor mixing ratio (contour at 3×10^{-4} kg·kg $^{-1}$), averaged between 6 and 9 km MSL (upper panels) and between 0 and 3 km MSL (lower panels). Labels “V1” and “V2” indicate the center of mid-level mesovortices. The surface vortex center and a 100-km radius from this are also indicated.

panels), there was a mesoscale convective system possessing a mid-level mesoscale vortex (labeled “V1”) to the southwest of the surface vortex center. At this time, winds in the middle troposphere were almost mono-directional in the inner core region. This flow pattern changed greatly 6 hours later (center panels), as the mid-tropospheric vorticity area R (highlighted by a bold broken line) reached to the inner core region. A new convective element possessing another mesovortex (labeled “V2”) developed in the vicinity of the surface vortex center. In the subsequent hour (1200 UTC, right panels), this convective element developed into a partial eyewall surrounding the surface vortex. It is noteworthy that the preexisting convective system disappeared and the mesovortex V1 became filaments of anomalous vorticity until this hour. These results show that the eyewall developed rapidly without undergoing the merger of pre-existing convectively-induced vorticity elements.

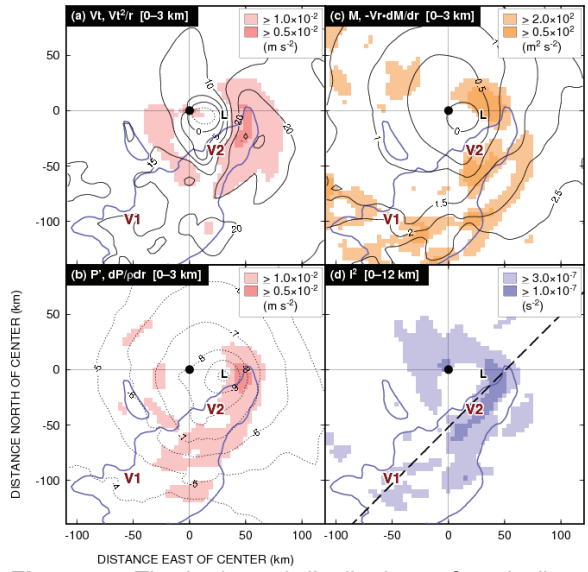


Figure 7. The horizontal distributions of vertically-averaged kinematic and dynamical parameters at 0600 UTC 18 June. (a) Tangential winds (contour, every 5 ms^{-1}) and centrifugal force (shaded). (b) Pressure anomaly (contour, every 1 hPa) and pressure gradient force (shaded). (c) Absolute angular momentum (contour, every $0.5 \times 10^6 \text{ m}^2 \text{ s}^{-1}$) and its radial advection (shaded). (d) Inertial stability parameter (shaded). Values in (a)-(c) are averaged between 0 and 3 km MSL while that in (d) is the mean value between 0 and 12 km MSL. Contours of negative value are drawn in dotted lines. Bold blue curves in all panels indicate the contour of hydrometeor mixing ratio ($> 3 \times 10^{-4} \text{ kg} \cdot \text{kg}^{-1}$, averaged between 0 and 3 km MSL). The center location of mid-level mesovortices V1 and V2 and the location of mid-level shearline R are superimposed.

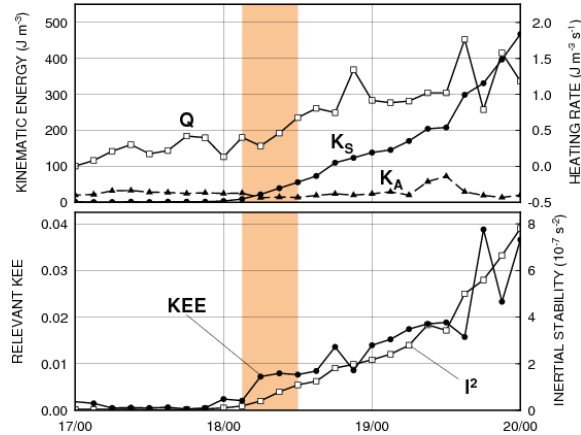


Figure 8. Time series of the diabatic heating rate (Q), axisymmetric (K_s) and asymmetric (K_a) kinetic energy, inertial stability (I^2), and relevant kinematic energy efficiency (KEE), calculated within 100-km range of the surface vortex and averaged between 6 and 9 km MSL.

The kinetic and dynamical features during the development of the mesovortex V2 are shown in Fig. 7. The developing convective element possessing V2 is marked by large horizontal gradient of tangential winds (as recognized from contours of Fig. 7a) and a pressure minimum (contours of Fig. 7b). These panels also show that the centrifugal force (Vt^2/r , color of Fig. 7a) was almost the same magnitude as the pressure gradient force ($\partial p/\partial r$, color of Fig. 7b) in and around the convective element. This means that the eye circulation in cyclostrophic wind balance began to form at this time near the developing partial eyewall. Figure 7c shows the area around V2 is also characterized by large horizontal gradient of absolute angular momentum ($M=rVt+fr^2/2$), due to inward radial advection of the angular momentum, suggesting the spin-up of circulation due to the low-level convergence associated with the partial eyewall.

5. EFFICIENCY OF INTENSIFICATION

Figure 7d shows high value of inertial stability [$I^2=(f+\zeta)(f+2Vt/r)$, ζ is relative vorticity] in the vicinity of the convective element. The increase in the inertial stability in the middle to upper troposphere was partly attributed to the increase in relative vorticity due to the superposition of the mid-tropospheric vortex R. The increase in inertial stability leads to stronger resistance to parcel displacement in the radial direction, which allows for greater efficiency in the dynamic response to convective heating (Schubert and Hack 1982). Nolan et al. (2007) pointed out that the kinetic

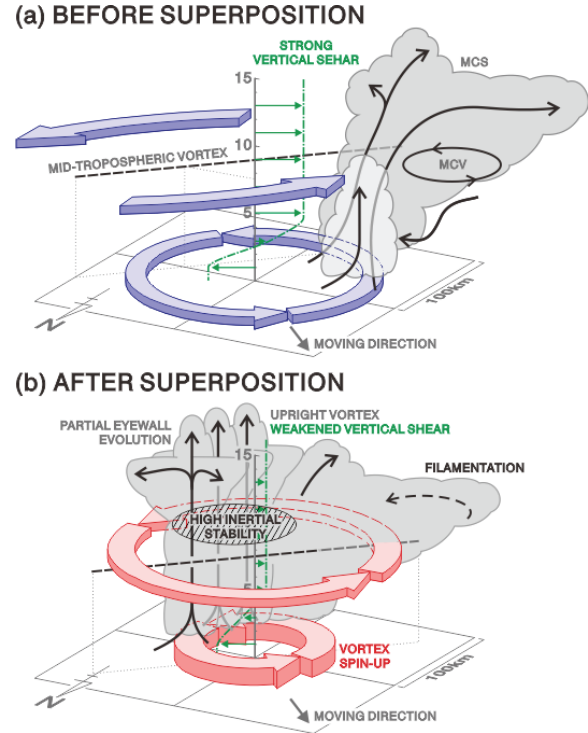


Figure 9. Schematic illustrations of the three-dimensional flow structure (viewing from northwest) before and after vortex superposition during the genesis of Typhoon Fengshen (2008).

energy efficiency (KEE), defined as the ratio of symmetric kinetic energy (K_s) to injected heat energy (Q), increases proportionally as the increase in inertial stability. To confirm this point in the present simulation, the volume-averaged relevant KEE in the middle troposphere was calculated and its change in time is shown in Fig. 8. As expected, the relevant KEE began to increase during the period of vortex transformation (0300–1200 UTC 18 June), with the increase in the inertial stability. This suggests that the convective element developing after the vortex superposition contributed to the spin-up of the pre-Fengshen surface vortex.

6. SUMMARY AND DISCUSSION

The multiscale processes leading to the genesis of Typhoon Fengshen (2008) were examined based on both the PALAU observation and NICAM simulation. Both of the observation and simulation provided a consistent feature that there were two separated vortices in different height before the genesis. The NICAM succeeded to reproduce the synoptic-scale evolution, characterized by the surface vortex beginning to develop just after the superposition of the mid-

tropospheric vortex. A close inspection of convective-scale processes near the surface vortex revealed that the spin-up of vortex with pressure fall started when a partial eyewall developed near the surface vortex center. The superposition of mid-level vortex contributed to the increase in inertial stability in the middle troposphere, providing higher efficiency in the dynamic response to diabatic heating by the partial eyewall. The force balance in the inner core region shifted from gradient-wind to cyclostrophic balance just after the superposition, and the surface vortex subsequently developed into a typhoon. These results, summarized as schematic illustrations in Fig. 9, show the crucial role of vortex superposition on the genesis of Fengshen.

One of the noteworthy points of this case is the spin-up of the surface vortex with the rapid development of a partial eyewall in the downwind side of a pre-existing mesoscale convective system. This development occurred under a rapid decrease in vertical wind shear due to the vortex superposition (not shown). This process is quite different from that simulated by Montgomery et al. (2006), in which the main vortex developed gradually through the merger of convectively-induced vorticity elements. In their idealized simulation, the vertical axis of main vortex already stands upright at the initial time. The results of our simulation suggest that the merger of convective-scale vortices is not always a necessary process for tropical cyclogenesis, especially under an influence of two or more synoptic-scale vortices.

Another point to be addressed is the origin of the two synoptic-scale vortices. From an analysis using the ECMWF—YOTC operational data (not shown), it is found that the surface vortex initially propagated westward along 5°N and turn to northwestward near 140°E while the mid-level vortex propagated westward in latitude of 10–15°N. The track of the surface vortex is quite similar to that of a tropical depression (TD)-type disturbance, usually transformed from mixed Rossby-gravity (MRG) wave along the equator (e.g. Dickinson

and Molinari 2002). It is hypothesized that the Fengshen case is an example of tropical cyclogenesis from such a TD-type disturbance. Composite analyses by Takayabu and Nitta (1993) showed that a tilted structure of MRG wave becomes upright during transformation into a TD-type disturbance. Therefore, it is suggested that observations of the vertical structure of each synoptic-scale vortex with high repetition frequency (less than half day) is important for further understanding of tropical cyclogenesis in the western tropical Pacific.

References

- Dickinson, M. and J. Molinari, 2002: Mixed Rossby-gravity waves and western Pacific tropical cyclogenesis. Part I: Synoptic evolution. *J. Atmos. Sci.*, **59**, 2183–2196.
- Fu, B., T. Li, M. S. Peng, and F. Weng, 2007: Analysis of tropical cyclogenesis in the western North Pacific for 2000 and 2001. *Wea. Forecasting*, **22**, 763–780.
- Mapes, B. E. and J. Lin, 2005: Doppler radar observations of mesoscale wind divergence in regions of tropical convection. *Mon. Wea. Rev.*, **133**, 1808–1824.
- Montgomery, M. T., M. E. Nicholls, T. A. Cram, and A. B. Saunders, 2006: A vortical hot tower route to tropical cyclogenesis. *J. Atmos. Sci.*, **63**, 355–386.
- Nolan, D. S., Y. Moon, and D. P. Stern, 2007: Tropical cyclone intensification from asymmetric convection: Energetics and efficiency. *J. Atmos. Sci.*, **64**, 3377–3405.
- Satoh, M., T. Matsuno, H. Tomita, H. Miura, T. Nasuno, and S. Iga, 2008: Nonhydrostatic Icosahedral Atmospheric Model (NICAM) for global cloud-resolving simulations. *J. Comput. Phys.*, **227**, 3486–3514, doi:10.1016/j.jcp.2007.02.006.
- Schubert, W. H. and J. J. Hack, 1982: Inertial stability and tropical cyclone development. *J. Atmos. Sci.*, **39**, 1687–1697.
- Sobel, A. H., and C. S. Bretherton, 1999: Development of synoptic-scale disturbances over the summertime tropical Northwest Pacific. *J. Atmos. Sci.*, **56**, 3106–3127.
- Takayabu, Y. N. and T. Nitta, 1993: 3–5 day-period disturbances coupled with convection over the tropical Pacific Ocean. *J. Meteor. Soc. Japan*, **71**, 221–246.